Effect of impurity mass on the microstructure of rapidly quenched aluminium

1993 J. Phys.: Condens. Matter 5 6139

(http://iopscience.iop.org/0953-8984/5/34/002)

J. Phys.: Condens. Matter 5 (1993) 6139–6148. Printed in the UK

Effect of impurity mass on the microstructure of rapidly quenched aluminium

V S Stepanyuk†, A Szasz‡, A A Katsnelson†, O V Wolf†, E Gyarmati§ and G M Kalibaeva†

† Department of Solid State Physics, Moscow State University, Lenin Hills, Moscow 117234, Russia

‡ Department of Atomic Physics, Eotvos University Budapest, Muzeum krt. 6–8, Budapest, H-1088, Hungary

§ Jülich Forschungszentrum, Institute of Reactor Materials, Jülich GmbH, Postfach 1913, W-5170 Jülich, Federal Republic of Germany

Received 27 August 1992, in final form 7 May 1993

Abstract. The microstructure of amorphous Al is investigated by molecular dynamics simulation. An unexpected mass effect caused by impurities is observed, which indicated the importance of the mass differences of components in generating the actual structure. Impurities with considerably lower masses than Al give amorphous microstructures, while much larger masses generate quasi-crystalline-like microstructures in the alloy. Both the Voronoi analysis and the pair correlation function are studied to clarify this effect.

1. Introduction

The effect of metalloids on the amorphous structure of metals is a well studied [1] topic in condensed-matter physics. On the microstructural level, metalloids promote fivefold clustering in the system [2] (first, distorted Frank–Kasper polyhedra [3] are preferred [4]), which is not consistent with the proper translation symmetry of the crystalline structures; the long-range order (LRO) has been broken. The loss of LRO emphasizes the role of short-range order (SRO) and medium-range order (MRO), which determine the amorphous matter [5]. The icosahedral microstructure (or other fivefold microstructures) may be arranged so strictly that a quasi-translation symmetry appears (quasi-crystals [6]) or may even be so disoriented (concerning of course SRO, since the disorientation starts from the second coordination sphere) that the structure may be said to be entirely amorphous.

On the other hand, microstructures depend greatly on the metalloid concentration [7] or else on the other metallic components [8]. In general the alloying elements considerably deform the matrix of the basic material, playing a decisive role in the non-crystalline micro-arrangements.

In our present paper we shall try to clarify the mass effect of the impurities introduced into the base material. This effect has not been regarded as relevant up to now (the chemical, electronic and size effects have mostly been studied), but our experience with clustering problems focused our attention on this 'side' effect.

One of the most investigated model systems is aluminium-based alloys, which generate various icosahedral phases and microstructures [9]. Consequently aluminium alloys were chosen for our present study.

0953-8984/93/346139+10$07.50

Earlier we have observed a marked concentration dependence of the microstructures on the alloying elements [10]. A very high concentration of the metalloids was required to observe amorphization in experiments by rapid cooling; so our interest was at first focused on the following questions.

(i) Does the interaction between impurities play a decisive role?

(ii) Does the size misfit and the chemical interactions create the observed non-crystalline structure?

(iii) Is it possible to obtain considerable microstructure changes by impurities without modifying the atomic sizes and pair potential?

2. Method

In order to study the above questions, we simulated the aluminium host by molecular dynamics (MD), modelling an ideal impurity in the system, which has the same size and interatomic potential as Al atoms, except that its mass may be different. The impurity mass dependence of the micro-arrangements in this system is investigated in the following.

Our MD calculation has been performed in the microcanonical ensemble NVE framework, where the energy E, the volume V and the number N of particles were kept constant in the averaging process of the physical data. Details have been published elsewhere [11]. The motion of 256 atoms is considered for the system which includes one impurity atom with a special mass, but all the parameters of this impurity were the same as for aluminium. This relatively small number of atoms is characteristic of the radial distribution function and is sufficient for the Voronoi analysis [12]; consequently, simple computers and a relatively short computing time can be used. The essential behaviour does not change on increase in the number of particles (we implemented up to 1000).

In the initial state the atoms were arranged in the nodes of a FCC lattice in a cubic box with edge L, and their velocities were assumed to be in accordance with a Maxwellian distribution at a temperature of 2000 K. The volume of the box is calculated from the experimental density of the aluminium. The well known periodic boundary condition was used.

A Morse-type empirical potential was applied for the interatomic interaction with a set of experimental parameters [13].

The integration of the motion equations was performed using a so-called 'leap-frog' algorithm [14] with a time step of 10^{-15} s. The system was stabilized at the initial temperature (2000 K) for 3000 steps to reach the standard liquid state. Starting with the well established equilibrium, the system was cooled in the next 10 000 steps (average rate of cooling was 10^{14} K s^{-1}) up to 300 K by rescaling the velocities of every particle by multiplying by a constant factor after every ten steps. After every 3000 time steps the alloy was thermally stabilized, and the thermodynamic and structural characteristics averaged with a correction of the system to the Maxwellian distribution at the actual temperature. These corrections were necessary to keep the system in a real thermodynamic process and allows enough time to create the relevant SRO. This is the reason that, despite the high cooling rate, the simulation is realistic and comparable with the experiments. The total process consisted of a sequence of cooling, stabilizing and averaging of some intermediate temperatures ranging from 2000 to 300 K in the cooling process of the system from the melt to the amorphous state. The glass transition temperature was identified by a sudden decrease—by several orders of magnitude—in the self-diffusion coefficient.

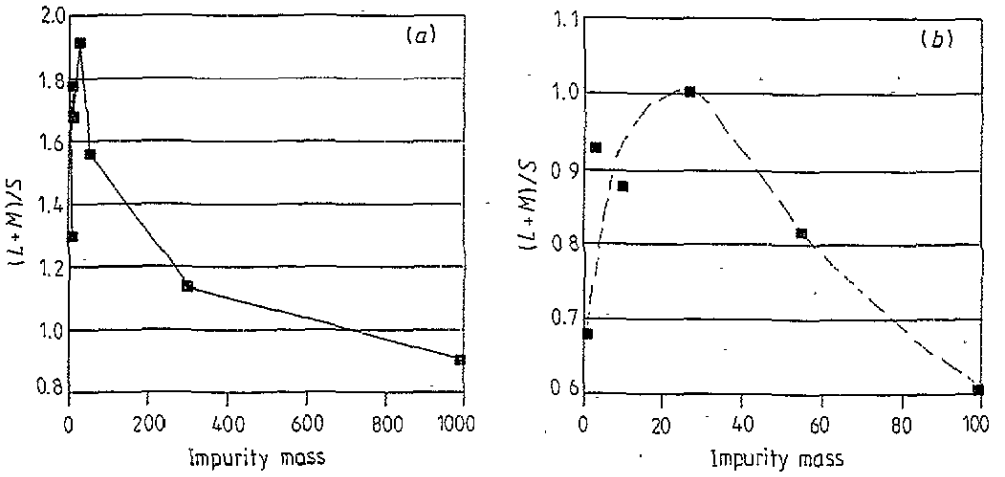

Figure 1. Voronoi analysis of rapidly quenched aluminium containing impurities with various masses. The ratio $(L+M)/S$ is given versus the impurity mass: (a) large-scale mass changes; (b) enlargement of (a).

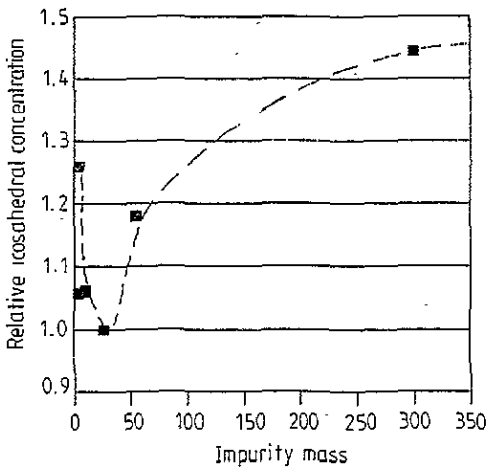

Figure 2. The impurity-mass dependence of the number of icosahedral arrangements ((00120) and (01102) polyhedra) in rapidly quenched Al.

The atomic positions after the above thermodynamic process were recorded; this enables the micro-arrangements, the correlation of the neighbours and their coordination clustering in the system to be studied. The radial distribution function (RDF) (partial pair correlation function $g_{ij}(r)$) was calculated parallel to recording the micro-arrangements.

Clustering is studied by the so-called Voronoi analysis which is a statistical analysis of the generalized Wigner–Seitz cells (Voronoi polyhedra [15]). To construct a polyhedral environment, every atom is assumed to be central, and the radii connecting this atom to its nearest neighbours were bisected by planes. These planes form the Voronoi polyhedron (like

the Wigner–Seitz cells in crystals) which is the geometrical dual of the actual coordination polyhedron.

In the evaluation of the polyhedral distribution we used the well known Schläfli notation [16], counting the edges of the faces and setting them in increasing order. In this way a polyhedron is denoted by a set of indices n_3, n_4, n_5, n_6, n_7, $\{n_i\}$, where n is the number of faces with vertices i. Consequently the Voronoi polyhedron of the BCC structure would be denoted by (0608), because its numbers of three-, four-, five- and six-edged polygons are 0, 6, 0 and 8, respectively. The Voronoi polyhedra of the FCC structure are rhombododecahedra, having 12 equal rhombuses as their faces; so their Schläfli notation is (0 12 0 0). (This is identical with the symbol for the HCP Voronoi polyhedron, indicating that the symmetries are not included in the notation—only the number of the surface polygons.) The icosahedral arrangement has a dodecahedron as its Voronoi polyhedron; so its symbol is (0 0 12 0). (Note that every dodecahedron (not only the regular dodecahedron) has this notation!) The statistics of the actual state of the phase contain all the types of Voronoi polyhedron realized in the actual state, and their frequency is also calculated around both the constituents. Highly deformed polyhedra also appeared. The well known periodic structures have various deformed intermediate polyhedra, such as (0364), (0365), (0446), (0447) and similar structures, which are generated from the distribution of the regular crystalline arrangements.

Table 1. The statistics of Voronoi polyhedra for various impurities in aluminium. Pure aluminium is given as a reference.

Impurity mass m (au)	Voronoi statistics				
	Icosahedra (%)	Prism (%)	FCC (%)	BCC (%)	Miscellaneous (%)
1	34.5	20.8	21.6	0.0	23.1
3	29.0	19.6	20.1	0.4	30.5
10	29.1	22.1	27.9	1.6	19.3
27[a]	27.4	20.2	24.7	0.8	26.9
55	32.3	17.3	20.0	1.6	28.8
300	39.6	15.3	26.0	1.2	17.9
1000	41.2	21.6	17.3	1.2	18.7

[a] This is the reference datum for pure aluminium.

3. Results and discussion

There are some characteristic differences in the distribution of the Voronoi polyhedra (symmetries in the first coordination spheres) of the system including various impurity masses (table 1). The Voronoi analysis of the microclusters shows an interesting distribution of the polyhedra in the system with the impurity, compared with pure aluminium (rapidly quenched in the same way as the other systems). As we described above, the Voronoi polyhedral analysis does not include symmetries in the Schläfli notation, but by the statistics of the characteristic polyhedra a symmetry characterization is available. If the number L of clusters corresponding to the proper LRO, the number S of polyhedra corresponding to the most characteristic SRO and the number M of microstructures between these structures

(mesoscopic effects and distorted polyhedra) are computed, then the $(L+M)/S$ ratio, is the largest for pure Al (figure 1). What is unexpected, however, is that this parameter decreases in both directions of changes in impurity mass. (The same effect is also observable for the icosahedral arrangements ((0 0 12 0) and (0 1 10 2)) alone (figure 2).

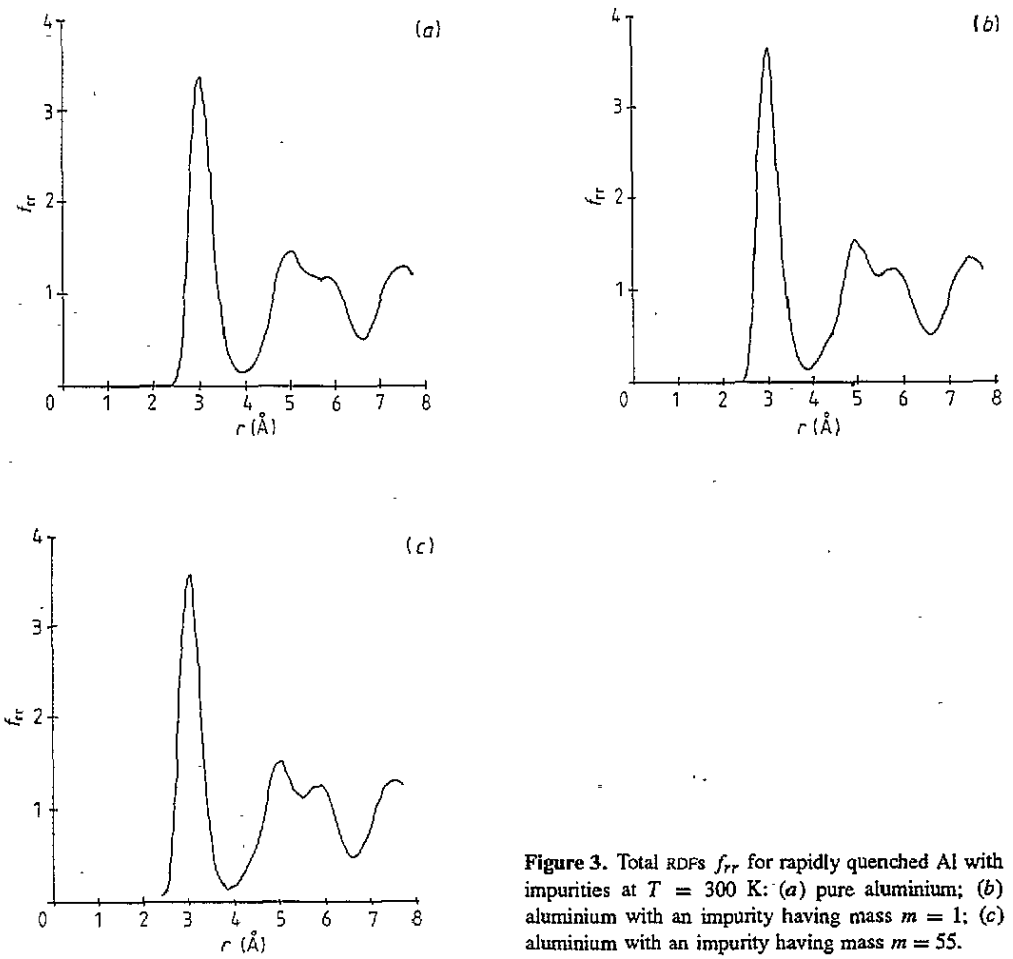

Figure 3. Total RDFs f_{rr} for rapidly quenched Al with impurities at $T = 300$ K: (*a*) pure aluminium; (*b*) aluminium with an impurity having mass $m = 1$; (*c*) aluminium with an impurity having mass $m = 55$.

The RDF provides information about the actual average distribution of the particles. The first peak corresponds to the hard-sphere radii, while its second (doublet) peak mirrors much more the actual micro-arrangements. The doublet refers to the second and third coordination spheres, contrary to the Voronoi polyhedra which correspond only to the nearest neighbours. The first subpeak of the RDF doublet—considering the atoms as hard spheres—agrees with the tetrahedral clustering ($r_t = 3\frac{2}{3}\sqrt{6} \simeq 4.90$), while the second corresponds to the collinear arrangements ($r_t = 3\times 2 = 6.00$) in the disordered system [17]. Moreover the plane structure consisting of two regular triangles ($r_\Delta = 3\sqrt{3} \simeq 5.20$), as well as the regular octahedron ($r_O = 3\sqrt{2} \simeq 4.25$), may also exist in this region [18]. Some characteristic distances for hard spheres and for regular polyhedra have been collected in table 2. The peaks are smeared because of the deformed polyhedra and the non-hard-sphere packing. The soft potentials shift the peaks towards smaller values.

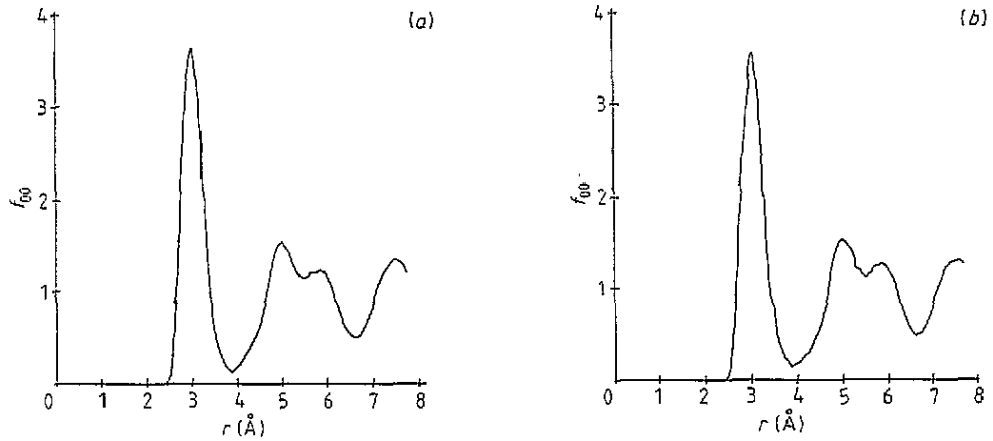

Figure 4. Partial Al–Al RDFs f_{00} for rapidly quenched Al with impurities at $T = 300$ K: (*a*) aluminium with an impurity having mass $m = 1$; (*b*) aluminium with an impurity having mass $m = 55$.

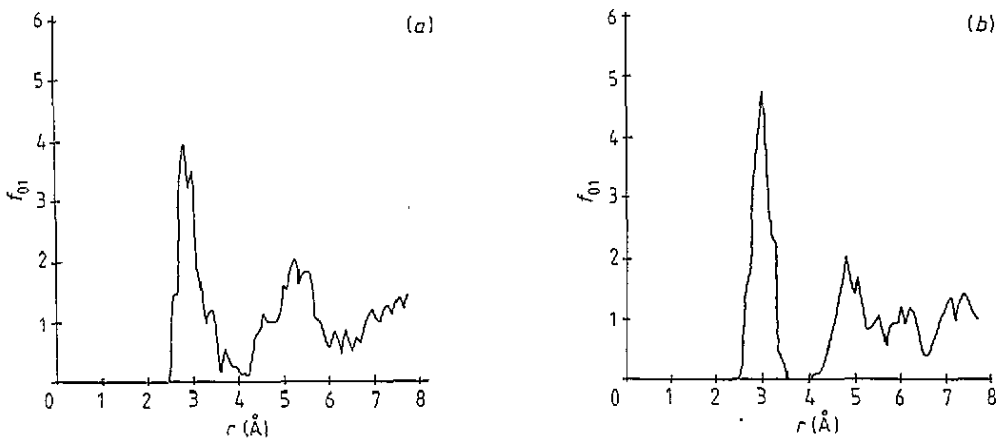

Figure 5. Partial Al–impurity RDFs f_{01} for rapidly quenched Al systems at $T = 300$ K: (*a*) aluminium with an impurity having mass $m = 1$; (*b*) aluminium with an impurity having mass $m = 55$.

The total RDF functions (figure 3) as well as the Al–Al bond distribution (figure 4) for pure Al and the systems containing impurities do not differ greatly; only a slight modification in the second peak-doublet intensity is observable, and the main difference is in the fine structure of the doublet. The pure aluminium has a hump between the subpeaks, which corresponds to the large number of octahedral arrangements in this material.

If we analyse the RDF data of the impurity–aluminium bonds (the distribution around the impurity), the curves in figure 5 show the markedly different characters of the systems with small and large impurity masses.

(i) The first peak of course remains at the same position, because the impurity has the

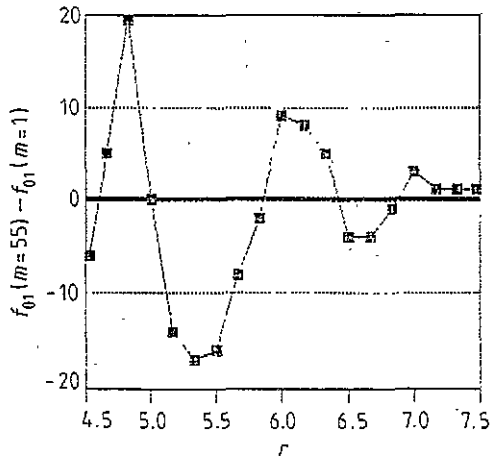

Figure 6. Difference between the partial RDF curves (difference between the curves shown in figure 5(*a*) and figure 5(*b*)) for the investigated systems.

same radius as Al.

(ii) The small-mass system prefers arrangements with $r_\Delta = 5.2$ in its second peak, while the large-mass systems are much more precisely characterized by the peaks at $r_1 = 4.9$ and $r_2 = 6.0$; so the doublet dominates the second peak of RDF only for large impurity masses.

The differences in the partial RDF curves (figure 6) demonstrate well the discrepancy caused by the masses alone.

The impurities locally disturb thermal equilibrium a great deal and so do the clustering processes. First of all, both the impurities locally disturb the equilibrium, thus emphasizing the role of the short-range effects. In this sense it does not matter whether the impurity mass m is larger or smaller than that of the base particles; in both cases the locally most optimal clustering will be arranged. The optimal clustering is icosahedral, or at least has fivefold symmetry [19], which is not affected by long-range (translation) symmetry requirements. This is the origin of the fact that the increase in the number of polyhedra characterizing short-range optimization was observed in both impurity mass classes of impurities (above and below the mass of aluminium).

On the other hand, the specific changes observed in the RDF can be explained by the differences in the mobility of the given impurity. The small-mass impurities (having the same average energy as the Al atoms) have a much higher velocity v than its neighbours, while the impurities with large masses have a much lower velocity. A high-velocity particle reaches a larger area during its motion than the average (Al), and of course the particles with low velocities influence a smaller area of the base material. However, impulses p of the particles, with the same kinetic energy, satisfy the conditions

$$p_1/p_2 = \sqrt{m}_1/\sqrt{m}_2$$
$$v_1/v_2 = \sqrt{m}_2/\sqrt{m}_1.$$

So, the impurity with a larger mass has a larger impulse and at the same time a smaller velocity than the average. Consequently, the large mass is relatively 'hot' in its neighbourhood and is able to transfer a larger impulse by scattering than the average. The

Table 2. Some characteristic distances of micro-arrangements built up by the regular polyhedra, and hard spheres. The radii of the spheres are unity.

Arrangement	Distance[a]
BCC edge	$2/\sqrt{3} \simeq 1.15$
Octahedron opposite vertices	$\sqrt{2} \simeq 1.41$
Icosahedron two triangles sharing one edge	$\sqrt{15}/(\sqrt{5}-1)/2 \simeq 1.56$
Two triangles in a sheet sharing one edge	$\sqrt{3} \simeq 1.73$
Prism (two tetrahedra)	$2\sqrt{6}/3 \simeq 1.63$
Octahedron with a tetrahedron sharing one face	$\sqrt{7}/\sqrt{2} \simeq 1.87$
Icosahedron opposite vertices	$(10+2\sqrt{7})^{-1/2} \simeq 1.90$
Collinear chain	2
Octahedron with two tetrahedra in its opposite face	$1/\sqrt{6}+2\sqrt{6}/3 \simeq 2.04$
Shortest distance in two FCC units	$\sqrt{5} \simeq 2.24$
Icosahedron with two opposite tetrahedra	$2\sqrt{6}/3+(42+18\sqrt{5})^{-1/2}/12 \simeq 2.39$
FCC diagonal	$\sqrt{6} \simeq 2.45$

[a] These values should be multiplied by the actual atomic-sphere radii r_a (which is in our case $r_a = 3$).

small impurity, however, is 'colder' than the average, exchanging smaller impulses in one scattering process with the Al particles. The vicinity of the large masses is 'heated', relaxing the lattice locally and creating icosahedral, prism-type and even FCC and BCC clustering. The small-mass impurity 'cools' the material but jumps quickly from cluster to cluster, creating 'open' arrangements in its neighbourhood; consequently it prefers connected triangles. On this basis the small-mass impurity has in its RDF a characteristic peak corresponding to the joined regular triangles, which share a common edge, both in their plane form (r_Δ) and also as a fraction of an icosahedral surface (r_s).

This simple scattering mechanism causes a characteristically different RDF around the impurities of various masses.

The small-mass impurity, because of its large effective scattering area and low impulse exchange, prefers amorphization of the material, creating more icosahedra than in pure Al. This is indeed observed when pure metals become amorphous owing to their hydrogen content.

On the other hand, large-mass impurities allow microregions to reach their optimal

arrangements, which are mostly icosahedral, but the vicinity of the impurity becomes more ordered (preferring large three-dimensional units) and supports the creation of quasi-crystalline order.

4. Conclusion

We observed different mechanisms of impurities in rapidly quenched aluminium, depending on the impurity mass relative to atomic mass of aluminium. The impurities with smaller masses than Al generate an amorphous structure, while impurities with relatively large masses support quasi-crystalline formation.

Acknowledgment

The authors wish to acknowledge the financial support from Inter-Rest Ltd, Hungary.

References

[1] Steeb S and Warlimont H (eds) 1985 *Proc. Int. Conf. on Rapidly Quenched Metals Proc. 5th Int. Conf. on Rapidly Quenched Metals* vols 1 and 2 (Amsterdam: Elsevier)
Proc. Int. Conf. on Liquid and Amorphous Metals e.g. 1992
(*8th Proc. Int. Conf. on Liquid and Amorphous Metals (Vienna, September 1992)*)
Physics and Chemistry of Finite Systems Proc. Int. Conf. on Quasi-crystals ed P Jena *et al* (1992 *Proc. 4th Int. Conf. on Quasi-crystals (Richmond, 1992)* (Deventer: Kluwer))
Elliot S R 1990 *Physics of Amorphous Materials* (London: Longman) (New York: Wiley)
Borisov M, Kirov N and Vavrek A (ed) 1989 *Disordered Systems and New Materials* (Singapore: World Scientific)
Stepanyuk V S, Katsnelson A A, Szasz A, Kozlov A B and Krasser W 1991 *Physica* B **169** 278
Szasz A, Kertesz L, Aysawy M A, Kirchmayr H, Muller H and Watson L M 1991 *J. Non-Cryst. Solids* **130** 211
Stepanyuk V S, Katsnelson A A, Kozlov A B, Farberovich O V, Szasz A and Kojnok J 1991 *Phys. Status Solidi* a **163** 139
[2] Stepanyuk V S, Katsnelson A A, Szasz A, Trushin O S and Nayak P 1990 *Phys. Status Solidi* b **122** K7
Stepanyuk V S, Szasz A, Katsnelson A A, Kozlov A B and Farberovich O V 1990 *Physica* B **164** 300
[3] Frank F C and Kasper J S 1958 *Acta Crystallogr.* **11** 184; *Acta Crystallogr.* **12** 483
[4] Stepanyuk V S, Szasz A, Katsnelson A A and Trushin O S 1991 *J. Non-Cryst. Solids* **130** 311
[5] Finney J L 1985 *Amorphous Solids and the Liquid State* ed N H March, R A Sreet and M Tosi (New York: Plenum) p 31
[6] Jaric M V (ed) 1988 *Introduction to Quasicrystals* vol 1 *Aperiodicity and Order* (New York: Academic)
[7] Stepanyuk V S, Katsnelson A A and Szasz A 1992 *Proc. Int. Conf. on Computational Physics (Prague, 1992)* (Abstract: 1992 *Phys. Comp.* **6** 303)
[8] Aysawy M A, Szasz A, Dankhazi Z, Hajdu J and Kertesz L 1991 *J. Non-Cryst. Solids* **127** 130
Belin E and Traverse A 1991 *J. Phys.: Condens. Matter* **3** 2157
Belin E, Dankhazi Z, Sadoc A, Calvayrac Y, Klein T and Dubois V M 1992 *J. Phys.: Condens. Matter* **4** 4459
Belin E, Kojnok J, Sadoc A, Traverse A, Hormalin M, Berger C and Dubois J M 1992 *J. Phys.: Condens. Matter* **4** 1057
[9] Shoemaker D P and Shoemaker C B 1988 *Introduction to Quasicrystals* vol 1 *Aperiodicity and Order* ed M V Jaric (New York: Academic) p 1
[10] Aysawy M A, Szasz A, Kertesz L and Dankhazi Z 1990 *J. Non-Cryst. Solids* **122** 146
[11] Stepanyuk V S, Katsnelson A A and Szasz A 1992 *Proc. 8th Int. Conf. on Liquid and Amorphous Materials (Vienna, 1992);* 1992 *Proc. Int. Conf. on Computational Physics (Prague, 1992)* (Abstract: 1992 *Phys. Comp.* **6** 326)

[12] Stepanyuk V S, Katsnelson A A, Szasz A and Trushin O S 1990 *Phys. Status Solidi* b **161** K77
Stepanyuk V S, Katsnelson A A, Szasz A, Trushin O S and Nayak P 1991 *Phys. Status Solidi* b **164** 395
[13] Lakkonen J and Nieminen R M 1985 *J. Non-Cryst. Solids* **75** 237
[14] Fincham D 1980 *Comput. Phys. Commun.* **21** 247
[15] Nelson D R and Spaepen F 1989 *Solid State Physics* vol 42 (New York: Academic) p 1
[16] Coxeter H S M 1947 *Regular Polytopes* (London: Methuen)
[17] Finney J L 1970 *Proc. R. Soc.* A **319** 479
[18] Bennett C H 1972 *J. Appl. Phys.* **43** 2727
[19] Hoare M R and Pal P 1971 *Adv. Phys.* **20** 161
Honeycutt J D and Andersen H C 1987 *J. Phys. Chem.* **91** 4950
Beck T L and Berry R S 1988 *J. Chem. Phys.* **88** 3910